INSTITUTE OF PHYSICS PUBLISHING JOURNAL OF MICROMECHANICS AND MICROENGINEERING

J. Micromech. Microeng. **14** (2004) 761–768 PII: S0960-1317(04)73408-7

Frequency-dependent bifurcation in electromechanical microfluidic structures

K-L Wang and T B Jones

Department of Electrical & Computer Engineering, University of Rochester, Rochester, NY 14627, USA

E-mail: jones@ece.rochester.edu

Received 15 December 2003
Published 19 April 2004
Online at stacks.iop.org/JMM/14/761 (DOI: 10.1088/0960-1317/14/6/001)

Abstract

Dielectric liquids rise up between vertically oriented, parallel electrodes if a voltage is applied. The resulting hydrostatic equilibrium balances the upward-directed ponderomotive force with the downward-directed gravitational force. Coating the electrodes with a dielectric layer makes it possible to achieve a similar, but now frequency-dependent effect with conductive liquids. If the electrodes (either coated or uncoated) are made slightly convergent, with the spacing closer at the top, the electric field coupled hydrostatic equilibrium exhibits a bifurcation. In this paper, a simple theory based on the Maxwell stress tensor and a linear RC circuit model is used to predict the frequency-dependent height-of-rise and the bifurcation phenomena. In the experiments, we used parylene-coated stainless steel electrodes, 24 mm long and 6.5 mm wide, to observe the height-of-rise of DI water and 1 mM KCl solution over the frequency range from 50 Hz to 20 kHz. The frequency-dependent experimental height-of-rise data, including the critical voltage and column height at which bifurcation occurs, are consistent with theoretical predictions. A simple model based on this theory successfully predicts the trapped liquid volume. Bifurcation phenomena have potential implications for the dynamic behavior of microfluidic schemes based on electrowetting and dielectrophoretic liquid actuation.

1. Introduction

The forces exerted on dielectrics and conductors by non-uniform electric fields can be exploited to transport and manipulate fluids ranging from electrically insulating liquids to aqueous electrolytes. Early demonstrations of the phenomenon with dielectric liquids were motivated by applications in spacecraft, for example, management of liquid propellant in low gravity [1] and the electrohydrodynamic heat pipe [2]. Much more recently, developments in the laboratory-on-a-chip and other microfluidic systems have reinvigorated interest in electric-field-based liquid management and control. This resurgence has focused on applications in biomedical research and microsystem cooling technologies, dictating a change from dielectric liquids to aqueous media, which are much more electrically conductive. In structures with dimensions larger than approximately a millimeter, the voltages and electric field strengths required to control aqueous liquids lead to unacceptable Joule heating; however, at smaller scales, electrical forces easily dominate over both gravity and capillarity, while surface-dependent conductive heat transfer helps limit temperature increases [3].

There are many ways to control a liquid using an electric field. One promising method utilizes the non-uniform electric field created by dielectric-coated, planar electrodes patterned on insulating substrates to control and manipulate sessile droplets and small volumes of aqueous liquid. Chief examples of such schemes are (i) electrostatic droplet transport [4–6], (ii) the electrowetting on dielectric (EWOD) effect [7–9] and (iii) dielectrophoretic (DEP) actuation [10, 11]. The dielectric coatings, ranging from $\sim$2 to $\sim$20 μm thick, prevent electrolysis and other detrimental water/metal interactions. The simple, open geometries of these systems afford good access to working surfaces, rapid actuation, and freedom from the leakage and channel-priming problems associated with closed channel microfluidic systems.

The subject of this paper is a bifurcation effect that influences the hydrostatic equilibria of moderately conductive

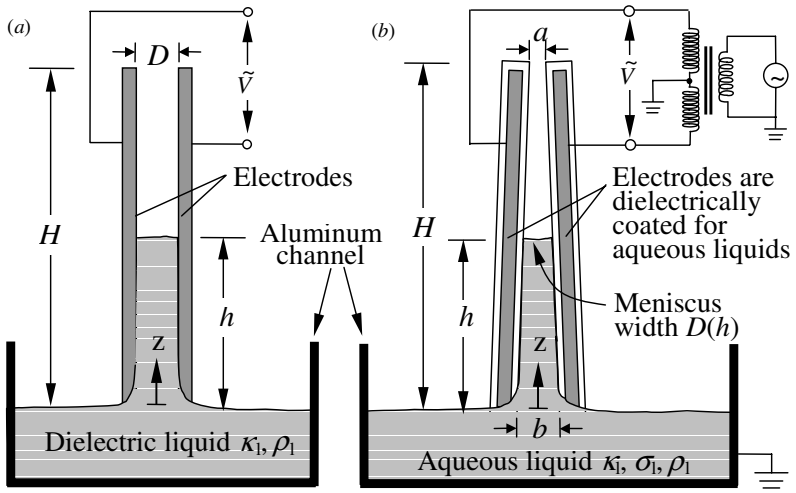

Figure 1. Height-of-rise experiments. (*a*) In Pellat's original experiment, an insulating liquid of dielectric constant κ_l and density ρ_l rises between two uncoated, vertical and parallel electrodes at spacing D dipped into a reservoir of liquid. (*b*) Modified apparatus for studying bifurcation uses slightly convergent electrodes spaced closer at the top. For experiments with aqueous liquids of finite conductivity σ_l, the electrodes are coated with a thin layer of dielectric constant κ_d and thickness $d \ll D$, and the reservoir is grounded; for dielectric liquids, the electrodes are uncoated and no ground connection is necessary. The voltage supply uses two series-connected, step-up transformers with the midpoint connected to the reservoir, thereby assuring application of balanced ac voltage to the electrodes with respect to the conducting liquid.

(aqueous) liquids actuated by the electromechanical force between vertically oriented, planar electrodes. The phenomenon, which depends on electric field frequency, can also be expected to affect steady and transient flow dynamics in some cases. Because of its possible effect on flow, bifurcation is potentially important in a range of microfluidic and liquid distribution applications where electromechanical actuation forces are exploited.

2. Background

More than one hundred years ago, Pellat showed that an insulating, dielectric liquid rises upward against gravity between two parallel electrodes when voltage is applied [12]. The electric-field-mediated hydrostatic equilibrium, shown in figure 1(*a*), exemplifies the ponderomotive force exerted on dielectrics by a non-uniform electric field [13]. If electrode spacing D is small compared to width w and height H, then the electric field between the electrodes becomes $E \approx V/D$, and the liquid height-of-rise h is [14]

$$h = \frac{(\kappa_l - 1)\varepsilon_0 E^2}{2\rho_l g} \tag{1}$$

where κ_l and ρ_l are, respectively, liquid dielectric constant and density, $g = 9.81$ m s^{-2} is the gravitational acceleration, and $\varepsilon_0 = 8.854 \times 10^{-12}$ F m^{-1} is the permittivity of free space. The derivation of equation (1) assumes that the space above the liquid is filled with some gas of negligible density and unity dielectric constant. It is important to note that the dielectric height-of-rise does not represent a pumping mechanism. Rather, it is analogous to the surface-tension driven rise of liquid in a capillary tube.

This hydrostatic equilibrium undergoes an interesting change if the electrodes are made to be slightly convergent, with the spacing at the top a smaller than at the bottom b as shown in figure 1(*b*). In particular, for dielectric liquids, if the spacing ratio $r = a/b < 2/3$, then $h(V)$ becomes a double-valued function over the range $0 < h < H$, signifying a bifurcation of the hydrostatic equilibrium [15]. One manifestation of this bifurcation is the spontaneous jump of the liquid from some critical point $z = h^*$ to the top of the structure, once the voltage is increased beyond a threshold value V^*. The other manifestation is observed if, with $V > V^*$ so that the liquid column fills the structure to the top, the voltage is reduced slowly. At $V = V^*$, the free interface collapses inward on both sides of the liquid column at $z = h^*$, trapping liquid at the top. Right at the condition for bifurcation, there exists an inflection in the hydrostatic equilibrium, above which no equilibrium—stable or unstable—exists. This is why the liquid meniscus spontaneously rises to the top when V exceeds V^*.

In this paper, we report experiments and describe a supporting model for bifurcation of the hydrostatic equilibrium for coated electrodes and somewhat conductive, aqueous liquids. The criterion for bifurcation, still expressed in terms of the ratio $r = a/b$, becomes dependent on frequency and liquid conductivity. We develop a simple electromechanical model adapted from earlier work [16–18] which uses the Maxwell stress tensor to predict the height-of-rise h versus voltage V and frequency f. Experimental data obtained with DI water and a KCl solution for ac voltages from 50 to 20 kHz conform closely to the predictions of this model in structures with spacing ratio covering the range $1/7 \leqslant r \leqslant 1/2$. In addition, the model successfully predicts the trapped volume of liquid.

3. Hydrostatic model

In the model, it is assumed that the electrode spacing $D(z)$ decreases linearly from b at the bottom to a at the top,

$$D(z) = b - \alpha z, \qquad 0 \leqslant z \leqslant H \tag{2}$$

where $\alpha = (b - a)/H$. The conditions $a < b \ll w \ll H$ assure that the electric field between the electrodes is quasi-uniform, that is, $E(z) \approx V/D(z)$. Furthermore, we assume that the uniform, insulating coating on the electrodes, of dielectric constant κ_d, is very thin, that is, $d \ll D$, thereby guaranteeing good accuracy for a linear RC circuit model introduced to determine the electric field distribution in the liquid and dielectric layers. The liquid has dielectric constant κ_l, electrical conductivity σ_l and density ρ_l.

3.1. Maxwell stress tensor

The hydrostatic equation for the liquid may be written as

$$-\nabla p - \rho_l g\hat{z} + \bar{f}^e = 0 \tag{3}$$

where p is the conventional hydrostatic pressure, $g = 9.81\ \mathrm{m\ s^{-2}}$ is the gravitational acceleration, and the electrical body force is expressed using the Korteweg–Helmholtz formulation [19, 20]:

$$\overline{f}^e = \rho_f \overline{E} - \frac{1}{2}E^2\nabla\varepsilon + \nabla\left(\frac{1}{2}E^2\rho\frac{\partial\varepsilon}{\partial\rho}\right). \tag{4}$$

The third term in equation (4) is electrostriction and has no effect if the liquid is incompressible [21]. In the Korteweg–Helmholtz formulation of the height-of-rise problem, all upward (z-directed) electrical force contributions are placed at the upper, horizontal liquid interface (the meniscus) between the electrodes. For this reason, it is convenient to use the Maxwell stress tensor to determine the electromechanical force [20]:

$$T^e_{mn} = \varepsilon E_m E_n - \delta_{mn}\tfrac{1}{2}\varepsilon E_k E_k. \tag{5}$$

Figure 2(a) shows the closed surface Σ encompassing the meniscus upon which the force balance is imposed. If the top and bottom surfaces of Σ are located, respectively, upward and downward from the gas/liquid interface, a distance much greater than d but much less than D, then the electric field is essentially tangential and all normal stress terms take the form $T^e_{zz} = -\frac{\kappa\varepsilon_o}{2}E^2_{tan}$. Evaluating the force this way incurs negligible error as long as $d \ll D(z)$ and $\alpha \ll 1$. Then, the z-directed force balance may be written as

$$\oint_\Sigma T^e_{zz}\,\mathrm{d}S + D(z)w(p_l - p_0) = 0. \tag{6}$$

Note that care must be taken to account properly for the signs of the stress tensor integral terms. According to the Korteweg–Helmholtz formulation, the pressure difference in equation (6) is determined solely by the static gravitational head. Thus,

$$p_l - p_0 = -\rho_l g h. \tag{7}$$

It is straightforward to add a surface tension contribution to equation (6); however, the electrode spacings in the experiments are large enough so that the electrical force completely dominates over capillarity, and so we ignore it to focus on the electromechanical effect.

The electric field quantities needed to evaluate the Maxwell stress terms in the integral of equation (6) are determined using an RC circuit model previously introduced for the case of parallel electrodes [17, 18]. Here, the electrode spacing is a slowly varying function of position and the meniscus width is $D(h) = b - \alpha h$. Nevertheless, as long as $\alpha \ll 1$, the circuit model is accurate. Using elementary voltage divider relations, we obtain

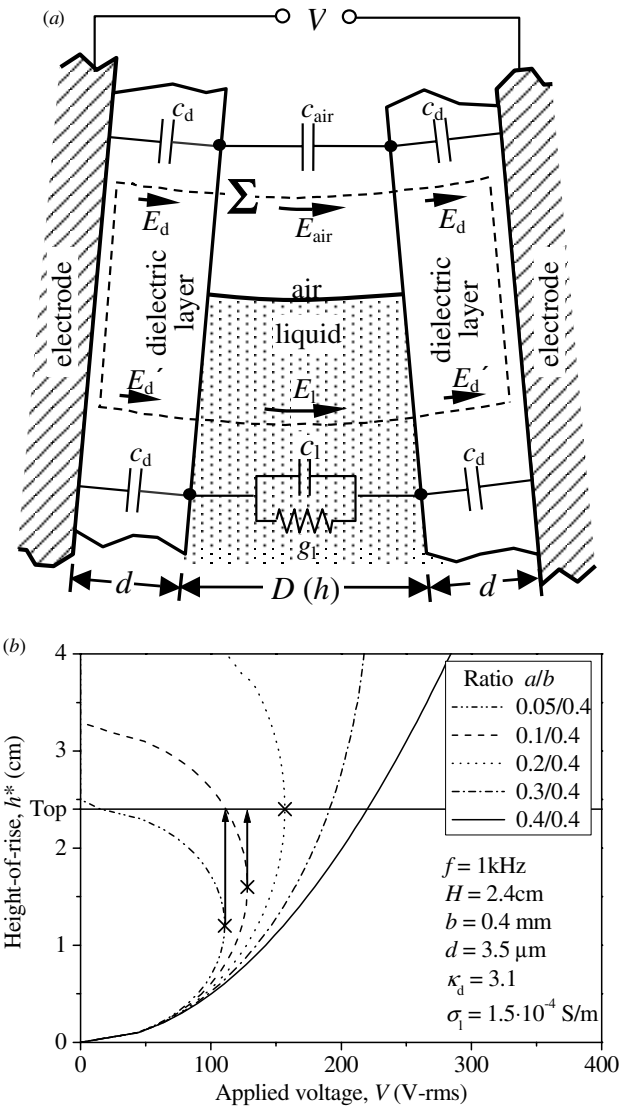

Figure 2. (a) Liquid meniscus showing closed surface Σ used for Maxwell stress tensor evaluation of electrical force and RC circuit model for evaluation of the electric field as a function of frequency. (b) Calculated height-of-rise h versus voltage V at 1 kHz. For this calculation, $H = 24$ mm, $b = 0.4$ mm and a ranges from 0.05 mm (convergent) to 0.4 mm (parallel). While $h(V)$ is always double-valued for convergent structures, i.e., $r = a/b < 1$, bifurcation occurs in the conductive limit only when $r < 1/2$ if the physical electrode length H is taken into account.

$$E_{air} = \frac{c_d}{2c_{air} + c_d}V/D(h) \tag{8a}$$

$$E_d = \frac{c_{air}}{2c_{air} + c_d}V/d \tag{8b}$$

$$E'_l = \mathrm{Re}\left[\frac{\mathrm{j}\omega c_d}{\mathrm{j}\omega(2c_l + c_d) + 2g_l}V/D(h)\right] \tag{8c}$$

$$E'_d = \mathrm{Re}\left[\frac{\mathrm{j}\omega c_l + g_l}{\mathrm{j}\omega(2c_l + c_d) + 2g_l}V/d\right]. \tag{8d}$$

The above expressions employ capacitance and conductance per unit area: $c_d = \kappa_d\varepsilon_0/d$, $c_{air} = \varepsilon_0/D(h)$, $c_l = \kappa_l\varepsilon_0/D(h)$

and $g_l = \sigma_l / D(h)$; V is rms voltage, $j = \sqrt{-1}$, and ω is the electrical frequency in radians per second.

An important crossover frequency is evident from examining equations (8*c*) and (8*d*):

$$\omega_c = \frac{2g_l(h)}{2c_l(h) + c_d} \tag{9}$$

For $\omega \ll \omega_c$, corresponding to the EWOD limit, the liquid behaves like a perfect conductor so that $E_l \approx 0$; below the liquid meniscus, most of the voltage drop occurs in the dielectric layer. On the other hand, $\omega \gg \omega_c$ corresponds to the DEP limit, in which case the liquid behaves like an insulator so that $\kappa_l E_l \approx \kappa_d E'_d$ [17].

Expressed in terms of the various electric field quantities, equation (6) takes the form

$$\varepsilon_0 w \left[-\kappa_d E_d^2 d - \frac{E_{air}^2}{2} D(h) + \kappa_d E_d'^2 d + \frac{\kappa_l E_l^2}{2} D(h) \right] - D(h) w \rho_l g h = 0. \tag{10}$$

Equation (10) combined with equations (8*a*)–(8*d*) provides the needed relationship between the height-of-rise h and the applied voltage V.

3.2. Predictions of the model

Figure 2(*b*) plots h versus V at fixed b for several values of the ratio $r = a/b$ between 1/8 and 1. Refer to the figure caption for the physical parameters used to obtain these curves. The solid line for $r = 1$ displays the usual quadratic dependence for parallel electrodes, that is, equation (1). On the other hand, $h(V)$ becomes double-valued when $r < 1/2$. The point on the curve where $dh/dV \to \infty$, that is, (V^*, h^*), represents a bifurcation of the equilibrium. If the voltage is increased to a value just above V^*, the liquid jumps up to the top of the structure, as indicated by the arrows. Note that, at fixed voltage, the reverse portion of the curve can never be observed. If, with the liquid column at the top of the structure, the voltage is then reduced slowly, at $V = V^*$ the liquid surface pinches inward from both sides at $z = h^*$, leaving a volume of liquid trapped at the top. While this behavior is quite similar to that described by Jones [15], in the present case, the coated electrodes and the conductive liquid introduce frequency dependence.

4. Experiments and phenomena

In the experiments, two 1 mm thick stainless steel electrodes ~25 mm long and ~6.5 mm wide were coated with parylene of thickness $d = 3.5$ (± 0.3) μm. These electrodes were mounted so that the angle and spacing between them could be adjusted independently. With this simple arrangement, the spacing ratio a/b could be varied from ~1/7 to ~1. Before taking measurements, a very thin film of insulating oil (Midel 7131) was wiped on the electrodes to abate stiction and wetting hysteresis. We used these oil-treated, parylene-coated electrodes for many individual experiments (>20), obtaining highly reproducible data without need for recoating. The electrodes were dipped into the reservoir liquid only ~1 mm to minimize parasitic resistance, which was found to cause an imbalance in the distribution of voltage on the two electrodes with respect to the grounded liquid.

Figure 1(*b*) shows the electrical circuit arrangements. AC voltage from a function generator (Leader model LG1301), amplified by a power amplifier (Krohn-Hite model DCA-50R), was supplied in parallel to two identical step-up transformers. By connecting the output windings in series, it was possible to maintain the liquid at ground potential through the metallic channel. This arrangement insured even distribution of the voltage between ground and the electrodes. We used an electronic counter (Fluke 1900A) and a true-rms multimeter (Fluke model 87), respectively, for frequency and voltage measurements.

The reservoir was made of a U-shaped channel cut from ~2 cm thick aluminum plate with glass plates glued to the front and back for observation. The height-of-rise was measured by a long-working distance stereo-microscope (Zeiss Stemi model SV6) equipped with a CCD camera; videos of the bifurcation phenomenon were recorded with a camcorder. Experiments were made with DI water and 1 mM solutions of KCl. Liquid conductivity σ_l, measured with a YSI conductance meter (model 35), ranged from 0.15 (± 0.03) mS m^{-1} for DI water to 140 (± 30) mS m^{-1} for 1 mM KCl solution. Measurements of trapped liquid volumes were made using standard capillary tubes of known internal diameter.

4.1. Bifurcation phenomena

The sequence of video images in figures 3(*a*)–(*f*) captures the essentials of the bifurcation. As shown in figure 3(*a*), the large spacing at the bottom (typically, $b > 0.5$ mm) guaranteed that capillary rise could be neglected. When voltage at frequency $f = 100$ Hz is applied, the liquid rises upward as shown in figure 3(*b*). Next in the sequence, figure 3(*c*) shows the liquid column at a point just below $z = h^*$. If the voltage is increased just slightly higher, the liquid rapidly and spontaneously jumps to the top within 2 video frames (at 30 frames per second), filling the structure as shown in figure 3(*d*). In these experiments, electric arcing is sometimes observed at the top. Voltages higher than ~300 V (rms) result in gas evolution due to electrolysis and liquid boiling, which deteriorates parylene coatings and affects experimental reproducibility.

Figure 3(*e*) reveals the bifurcation phenomenon that occurs when voltage is reduced slowly. At $V = V^*$, the free surface of the liquid column pinches in from both sides close to $z = h^*$, sometimes leaving a thin film. This film breaks after a time, especially if the voltage is decreased further. As a result, the liquid above $z = h^*$ is trapped, while a column is re-established at $h < h^*$ and a few very small droplets adhere to the electrodes in the open space between. If the voltage is reduced to zero and the electrodes then carefully separated, the trapped liquid forms a liquid bridge, evident in figure 3(*f*), that can be drawn off into a glass capillary tube for volume measurement.

The observed bifurcation effect is highly repeatable; however, once the liquid is trapped at the top, the liquid bridge it forms is supported by capillarity. The same kind of stable liquid bridge can be formed if a comparable liquid volume is injected there using a syringe. Even at the lowest ac frequencies, we see little evidence of electrical charging of the parylene coating, which might interfere with reversible behavior.

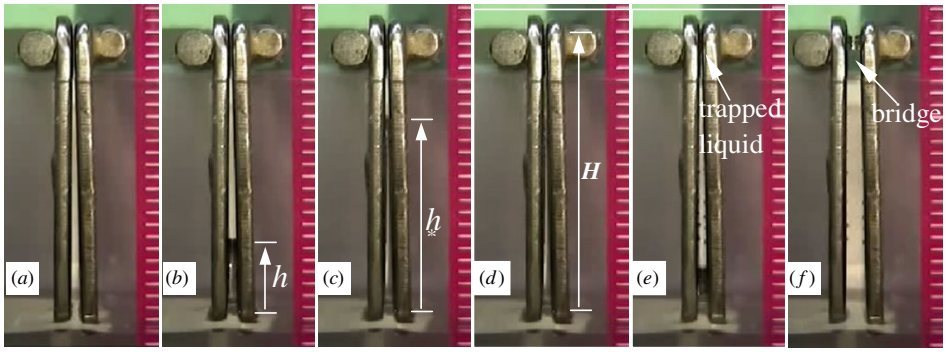

Figure 3. Sequence of images showing rise and fall of DI water between converging electrodes for increasing and decreasing voltage ($a = 0.2$ mm, $b = 0.8$ mm, $H = 24$ mm): (*a*) zero voltage, electrodes dipped ~1 mm into liquid with minimal capillary-induced height-of-rise; (*b*) liquid meniscus rises upon application of voltage; (*c*) liquid column height h close to bifurcation point h^*; (*d*) spontaneous rise of liquid column to the top after very small voltage increase; (*e*) failure of hydrostatic equilibrium on both open sides of column at $z = h^*$ upon decrease of voltage below V^*, with liquid trapped at the top; (*f*) liquid bridge near top of structure after removal of voltage and mechanical separation of electrodes.

5. Results

5.1. Frequency dependence of height-of-rise

Figures 4(*a*) and (*b*) plot measured height-of-rise versus voltage for DI water and 1 mM KCl solution at frequencies from 50 Hz to 20 kHz. The vertical arrows are used to signify the last *stable* equilibrium points before the observed jumps due to bifurcation. Predictions of the model based on equation (10) are plotted as continuous curves and correlate well with the data. For the experiment using DI water, the crossover frequency calculated using equation (9) is $f_c = \omega_c/2\pi = 14$ kHz (±2 kHz). Because this value is within the test range, DI water shows a dependence on frequency. In particular, note that h^* decreases with frequency. On the other hand, within the limits of measurement precision, the 1 mM KCl solution (cf figure 4(*b*)) exhibits no frequency dependence. We anticipate this result because, with conductivity almost one hundred times larger than that of DI water, the crossover of the KCl solution is ~1.3 MHz, far above the test range.

In experiments with both DI water and KCl solution, the measured voltage drops from 10 to 30 V (rms) after the spontaneous jump. Current loading of the transformers, precipitated by the four- to fivefold decrease in the net electrode to electrode impedance that accompanies the abrupt rise of the liquid, may explain this effect. Electrical breakdown in the dielectric layer may also contribute to current loading.

5.2. Saturation effects

The 50 Hz and 100 Hz data in figure 4(*a*), and other data for frequencies below ~1 kHz for DI water, exhibit a kind of saturation effect, where h deviates markedly from the predicted curves. This behavior is presumably the same *height-of-rise saturation* reported for parallel electrodes [18]. Welters and Fokkink also have observed this effect and showed a convincing correlation to contact angle saturation [7]. What is interesting and somewhat unexpected in our experiments with DI water at low frequencies is that, even when the height-of-rise is affected by saturation, bifurcation still manifests itself. It seems that the stronger electromechanical force, due to the more intense electric field near the top, somehow overwhelms any force clamping expected to result from contact angle saturation. One might conjecture that it is the rapid upward movement of the meniscus itself that overwhelms the influence of saturation on the electromechanical force.

5.3. Bifurcation voltage and height

As a further test of the model, we recorded values for the voltage and height-of-rise as close as possible to the bifurcation event for comparison to the model's predictions. Figure 5 is a composite of experimental data points for the critical voltage V^* versus values calculated using the parameters of each experiment for several values of spacing ratio r using DI water and the 1 mM KCl solution. The calculated values for V^* are obtained by using equation (10) under the condition $\mathrm{d}h/\mathrm{d}V \to \infty$. The measured values correlate well to predictions except in some cases at lower frequencies (<1 kHz), where the previously mentioned height-of-rise saturation effect intervenes, usually somewhere between 100 and 135 V. We find that bifurcation occurs in conjunction with saturation as long as V^* is no more than 20 ~ 30 V (rms) above the saturation threshold, a situation most likely at smaller electrode spacings. Figure 6 contains a similar plot for experimentally measured location of the bifurcation. That h^* is less influenced by saturation than V^* is consistent with the viewpoint that the bifurcation height is defined by purely geometrical considerations.

5.4. Trapped volume

Trapped liquid volumes were measured using capillary tubes of known inside diameter. A tube was inserted into the liquid bridge that forms after the voltage is turned off and the electrodes are mechanically separated. From observation, virtually all the liquid is taken up into the capillary tube apparently because the oil-treated parylene surface is slightly hydrophobic. The theoretical volume predictions used in the composite plot of figure 7 are calculated under the assumption that all liquid above the bifurcation point $z = h^*$ is trapped:

$$\text{Volume} = w(H - h^*)\left[\tfrac{1}{2}\alpha(H - h^*) + a\right]. \qquad (11)$$

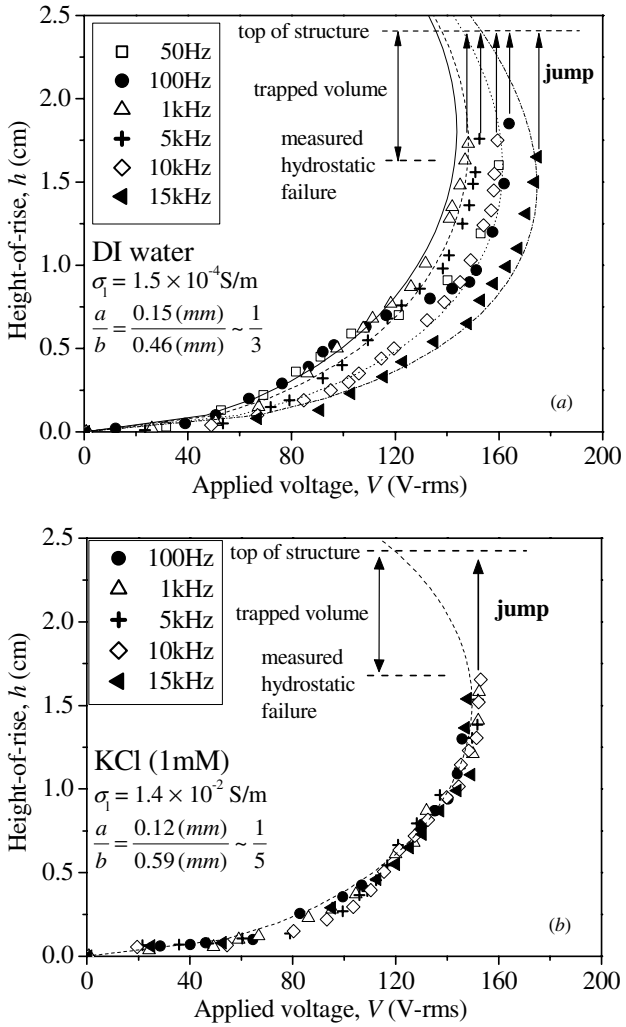

Figure 4. Height-of-rise h versus voltage V for frequencies ranging from 50 Hz to 20 kHz. The meniscus rises steadily until a critical point is reached, beyond which the column jumps spontaneously to the top as indicated by arrows. For clarity, some data points have been omitted. The continuous curves are predicted values from equation (10). (*a*) DI water (conductivity 1.5×10^{-4} S m^{-1}) with $a = 0.15$ mm, $b = 0.46$ mm, $H = 24$ mm. Deviations of the 50 Hz and 100 Hz data from predictions of the model for $V > \sim 120$ V (rms) are due to saturation. (*b*) 1 mM KCl solution (conductivity 1.4×10^{-2} S m^{-1}) with $a = 0.12$ mm, $b = 0.49$ mm, $H = 24$ mm. KCl data at all frequencies overlap because the crossover is two orders of magnitude higher than the highest test frequency.

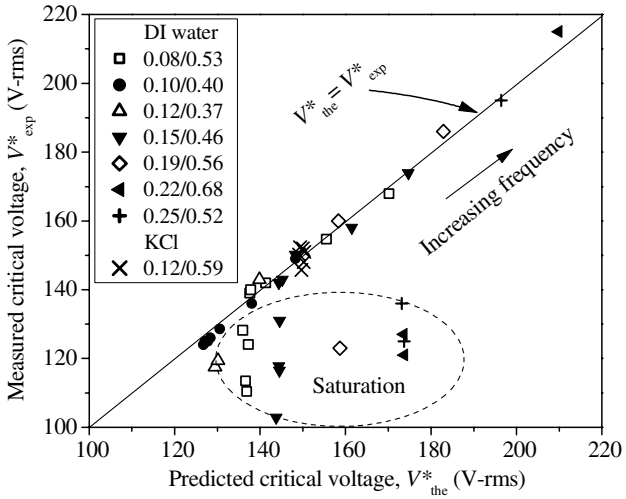

Figure 5. Composite plot of experimental bifurcation voltage data versus predicted values for V^*. In general, this critical voltage increases with spacing ratio and conductivity. At the higher frequencies (upper right), data are uniformly consistent with the theory. With DI water at lower frequencies, saturation sometimes occurs first, especially in structures with larger spacings.

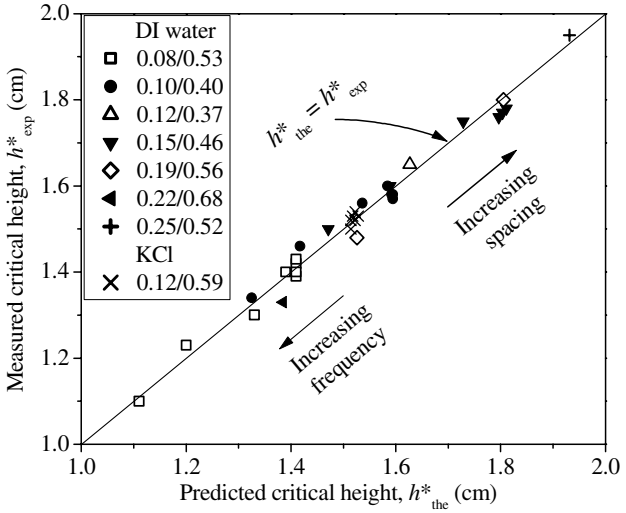

Figure 6. Composite plot of experimental bifurcation height data plotted versus predicted values for h^*. Within the measurement precision, the data are consistent with the theory, despite the fact that saturation sometimes occurs first before the bifurcation event.

Note that this volume depends on frequency by virtue of the frequency dependence of h^*. Deviations of measured trapped volumes from prediction may be due to a surface tension effect. When the pinch-in failure occurs at $z = h^*$, the thin film that forms and often persists after the voltage has been reduced, may drain some liquid back down into the reservoir.

6. Discussion

In parallel structures, the saturation effect imposes an upper limit on the elevation to which liquid can be raised [7, 18]. Thus, it is very interesting that, in non-parallel structures, the spontaneous jump of the liquid column to the top of the electrode structure can still occur—even when electromechanical saturation is encountered first. Refer to the 50 Hz and 100 Hz data plotted in figure 5(*a*). This intriguing result could be interpreted as an evidence that the saturation effect originates solely from electrowetting-induced changes in the solid/liquid interfacial profile, while the electromechanical height-of-rise, another observable, is a consequence of the net, upward-directed, force of electrical origin. This interpretation would be consistent with the correlation of electromechanical saturation to contact angle saturation [7]. The vigor of the spontaneous rise suggests that bifurcation offers a means to circumvent the limitations imposed by saturation. Its potential application in EWOD and DEP microfluidic schemes will require better understanding

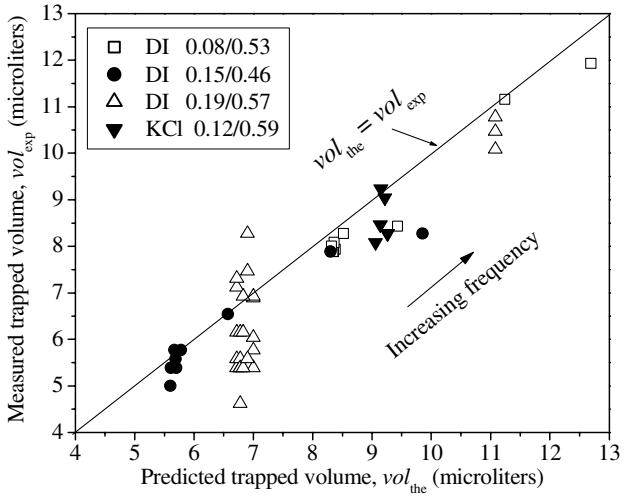

Figure 7. Composite plot of measured versus predicted trapped liquid volumes. The experimentally measured values are obtained using a capillary tube to draw off the liquid, while predicted values are calculated using equation (11). In some cases, the measured volume deviates by as much as 30% from the model, possibly because of liquid draining down from the top through a thin film. This film, the existence of which is probably related to surface tension, sometimes persists after the hydrostatic pinch-in failure has occurred.

of exactly how contact angle saturation interacts with this phenomenon.

Bifurcation has practical implications in microfluidic flows where the electromechanical force is used to effect liquid motion. One possible application is a micropump. As already stated, the electrohydrostatic equilibrium created by vertically aligned electrodes, parallel or non-parallel, coated or uncoated, is not intrinsically a pumping mechanism. When voltage is first turned on, the liquid rises in response, but this flow is transient; it slows down and comes to a stop as equilibrium is approached. On the other hand, if by some means trapped liquid is continuously removed from the top of the structure, then net flow may be realized. An example is the electrohydrodynamic (EHD) heat pipe, where evaporation continuously removes liquid at one end (and condensation returns it at the other end) [2]. In the EHD heat pipe, the energy sustaining this steady flow comes from the temperature difference, *not from the voltage source*. Bifurcation, as revealed in figure 3, offers another way to achieve net flow. By cycling the voltage on and off in spatially varying electrode structures, the voltage source provides the motive power as a consequence of the hysteretic nature of the liquid response. Consider the trapped liquid shown in figure 4(f), which has been raised against gravity and is now suspended entirely by surface tension *at zero voltage*. If this trapped liquid is removed by some means, for example, using a separate set of electrodes, before voltage is reapplied, then net flow is achieved. Such a mechanism could be the basis for a voltage-actuated, micromechanical pumping or precision metering scheme.

Other situations where bifurcation might be important are microfluidic devices using the electrowetting effect [7–9], in microelectronic cooling schemes [22], or in microfabrication processes where electrical forces are used to promote flow of encapsulant liquids into small gaps [23]. If electrode spacing is sufficiently non-uniform along the direction of flow, then the conditions for bifurcation may exist. The effect of non-uniform electrode spacing on flow failure of electromechanical flow structures has been observed in an electrohydrodynamic heat pipe [24].

An alternate scenario for bifurcation is a structure with constant electrode spacing D and spatially varying dielectric layer thickness, that is, $d(z)$. If the variation of d is large enough, such structures will exhibit bifurcation for conductive liquids. It should not be difficult to fabricate dielectric layers having controlled thickness profiles using sophisticated coating methods.

7. Conclusion

An electromechanical bifurcation effect has been investigated in vertically oriented, almost parallel electrodes. The bifurcation results in hysteretic behavior of the electrohydrostatic equilibria of the liquid. By coating the electrodes with thin dielectric layers, frequency-dependent bifurcation can be achieved with aqueous liquids of electrical conductivity up to $\sim 10^{-2}$ S m^{-1}. A simple electromechanical theory based on the Maxwell stress tensor and an RC circuit model to determine the electric field distribution successfully predicts the relationship between the height-of-rise and voltage, the critical voltage for bifurcation, and the height at which bifurcation occurs.

We measured the frequency dependence of the height-of-rise under ac voltages from 50 to 20 kHz and found that the data are consistent with the model's prediction for varied spacings and spacing ratios. In particular, we recorded the voltage and the location at which the liquid column spontaneously jumps to the top of the structure, and correlated these data to the model successfully. Also observed was the failure of the hydrostatic equilibrium when the voltage is slowly decreased from just above the critical value. The failure manifests itself as an inward collapse of the liquid surface at the critical height that pinches off part of the liquid column, trapping it at the top. Trapped liquid volumes were measured using standard capillary tubes and the resulting data generally agree with predicted values, if one assumes that all liquid above the bifurcation point is trapped. The experimental height-of-rise data reveal strong frequency dependence for DI water, but virtually none for 1 mM KCl solution. This is as expected because the crossover between the EWOD (low frequency) and DEP (high frequency) limits is $\sim$14 kHz for DI water and $\sim$1.3 MHz for the KCl.

Acknowledgments

A Clarke (Eastman Kodak Co) provided helpful comments on the bifurcation phenomenon as well as insights on electrowetting and dielectrophoresis. P Osborne fabricated the apparatus and L Chen assisted with some early experiments. All the parylene coatings were performed at the Semiconductor and Microsystems Fabrication Laboratory of the Rochester Institute of Technology with assistance from A Raisanen. The National Institutes of Health, the Center for Future Health of the University of Rochester, the National Science Foundation and the Infotonics Technology Center, Inc. (NASA grant no NAG3-2744) supported this work.

References

[1] Melcher J R, Hurwitz M and Fax R G 1969 Dielectrophoretic liquid expulsion *J. Spacecr. Rockets* **6** 961–7

[2] Jones T B 1974 An electrohydrodynamic heat pipe *Mech. Eng.* **96** 27–32

[3] Jones T B 2003 Electrostatics on the microscale, presented at *Institute of Physics Congress (Edinburgh, April)*

[4] Washizu M 1998 Electrostatic actuation of liquid droplets for microreactor applications *IEEE Trans. Ind. Appl.* **34** 732–7

[5] Torkkeli A, Saarilahti J, Häärä A, Härmä H, Soukka T and Tolonen P 2001 Electrostatic transportation of water droplets on superhydrophobic surfaces *IEEE/MEMS Conf. Technical Digest* pp 475–8

[6] Vykoukal J, Schwartz J A, Becker F F and Gascoyne P R C 2001 A programmable dielectrophoretic fluid processor for droplet-based processing *Micro Total Analysis Systems* ed J M Ramsey and A van der Berg pp 72–4

[7] Welters W J J and Fokkink L G J 1998 Fast electrically switchable capillary effects *Langmuir* **14** 1535–8

[8] Lee J, Moon H, Fowler J, Schoellhammer T and Kim C-J 2002 Electrowetting and electrowetting-on-dielectric for microscale liquid handling *Sensors Actuators* A **95** 259–68

[9] Pollack M G, Fair R B and Shenderov A D 2000 Electrowetting-based actuation of liquid droplets for microfluidic actuation *Appl. Phys. Lett.* **77** 1725–6

[10] Jones T B, Gunji M, Washizu M and Feldman M 2001 Dielectrophoretic liquid actuation and nanodroplet formation *J. Appl. Phys.* **89** 1441–8

[11] Ahmed R, Hsu D, Bailey C and Jones T B 2003 Dispensing picoliter droplets using DEP micro-actuation *Proc. Microchannels and Minichannels Conf. (ASME) (Rochester, NY, April)* pp 837–43

[12] Pellat H 1895 Mesure de la force agissant sur les diélectriques liquides non électrisés placés dans un champ élitrique *C. R. Acad. Sci., Paris* **119** 691–4

[13] Becker R 1982 *Electromagnetic Fields and Interactions* (New York: Dover) section 35

[14] Jones T B and Melcher J R 1973 Dynamics of electromechanical flow structures *Phys. Fluids* **16** 393–400

[15] Jones T B 1974 Hydrostatics and steady dynamics of spatially varying electromechanical flow structures *J. Appl. Phys.* **45** 1487–91

[16] Jones T B 2002 On the relationship of dielectrophoresis and electrowetting *Langmuir* **18** 4437–43

[17] Jones T B, Fowler J D, Chang Y S and Kim C-J 2003 Frequency-based relationship of electrowetting and dielectrophoretic liquid microactuation *Langmuir* **19** 7646–51

[18] Jones T B, Wang K-L and Yao D-J 2004 Frequency-dependent electromechanics of aqueous liquids: electrowetting and dielectrophoresis *Langmuir* **20** at press

[19] Landau L D and Lifshitz E M 1960 *Electrodynamics of Continuous Media* (Oxford: Pergamon) section 15

[20] Woodson H H and Melcher J R 1968 *Electromechanical Dynamics* (New York: Wiley) chapter 8

[21] Rosenkilde C E 1969 A dielectric fluid drop in an electric field *Proc. R. Soc.* A **312** 473–94

[22] Darabi J, Ohadi M M and DeVoe D 2001 An electrohydrodynamic polarization micropump for electronic cooling *J. Microelectromech. Syst.* **10** 98–106

[23] Tso C P, Sundaravadivelu K and Zhang L B 2004 Externally guided underfill encapsulation and subsequent filler particle migration during electronic packaging *J. Micromech. Microeng.* **14** 212–9

[24] Jones T B and Perry M P 1972 Experiments with an electrohydrodynamic heat pipe *Report to US National Aeronautics and Space Program (Ames Research Center)* NASA CR-114498